Earth, Planets and Space

EXPRESS LETTER

Open Access

Dynamically triggered seismicity in Japan following the 2024 M_w7.5 Noto earthquake

Like An[1*], Bogdan Enescu[1,2], Zhigang Peng[3], Masatoshi Miyazawa[4], Hector Gonzalez-Huizar[5] and Yoshihiro Ito[4]

Abstract

On January 1st, 2024, a moment magnitude (M_w) 7.5 earthquake occurred on an active reverse fault in the northern part of Noto Peninsula, being one of the largest intraplate events recorded in Japan. In previous studies, the dynamic triggering of seismicity in Japan following some large remote earthquakes has been well documented, such as in the case of the 2011 M_w9.0 Tohoku–Oki earthquake, the 2016 M_w 7.1 Kumamoto earthquake, and other large teleseismic events. In this study, we investigate the remote triggering of microearthquakes by the 2024 Noto earthquake and their characteristics. We analyze waveform data recorded at high-sensitivity seismic stations in Japan, before and after the occurrence of the Noto mainshock. Local earthquakes are detected on high-pass filtered three-component seismograms. Low-pass filtered waveforms are used for visualizing the mainshock surface waves and estimating dynamic stresses. Our results show a relatively widespread activation of small earthquakes—none of them listed in the Japan Meteorological Agency (JMA) earthquake catalog—that were triggered by the passage of the mainshock surface waves in many regions of Japan. These include Hokkaido and Tohoku in northeastern Japan, Kanto in central Japan, and Kyushu in southern Japan. The triggering is mostly observed in volcanic regions, supporting the hypothesis that such places are relatively easy to be activated dynamically, likely due to the excitation of fluids by the passage of mainshock surface waves. The calculated dynamic stress changes estimated from peak ground velocities, which triggered the earthquakes after the Noto mainshock, are in the range 12.8–102.6 kPa. We also report potential, less well-constrained dynamic triggering by the M_w 5.3 Noto foreshock, which occurred ~ 4 min before the mainshock, at levels of stress about 100 times smaller. The analysis of a longer-term (1 month) seismicity pattern, based on the JMA catalog, revealed a statistically significant increase of seismicity in the remote Akita–Yakeyama (Tohoku region) volcanic area, following the Noto earthquake.

Keywords Seismicity, 2024 Noto earthquake, Earthquake remote triggering, Dynamic stress changes

*Correspondence:
Like An
like.an.65h@st.kyoto-u.ac.jp
Full list of author information is available at the end of the article

Graphical Abstract

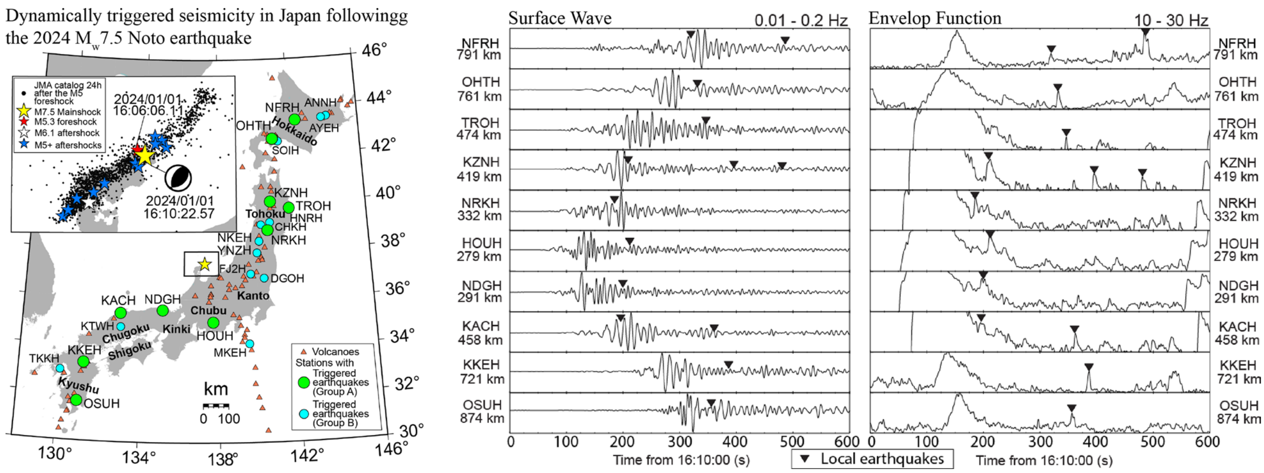

1 Introduction

After the occurrence of a large earthquake, many smaller events are reported to occur along the same fault as the mainshock or along neighboring seismogenic areas. These events, usually known as aftershocks, are mostly attributed to the triggering by static stress changes caused by slip on the mainshock fault (King et al. 1994), mainshock dynamic stress changes (Gomberg et al. 2001), or aseismic slip following the mainshock rupture (Perfettini and Avouac 2004). In some cases, triggered earthquakes are reported at distances larger than a few fault-lengths from the mainshock. At such remote distances, the static stress changes are too small to trigger seismicity, thus another mechanism is required to explain the seismicity activation. Many studies have confirmed that the passage of surface waves from relatively large earthquakes trigger dynamically seismicity, at areas located as far as hundreds to thousands of kilometers away from the mainshock (e.g., Hill et al. 1993; Brodsky et al. 2000; Hough et al. 2003; Gomberg et al. 2004; Velasco et al. 2008; Miyazawa 2011; Yukutake et al. 2013; Aiken and Peng 2014; Wang et al. 2015, 2018; Enescu et al. 2016; Opris et al. 2018; Fan et al. 2020; Takeda et al. 2024; Yao et al. 2015, 2024). In few cases, body waves were also reported as being capable of triggering earthquakes (e.g., Gomberg et al. 2004; Miyazawa 2012).

While the responsible physical mechanisms for the remotely triggered seismicity are still under debate, two sets of models are usually considered: (1) triggering by frictional failure and (2) triggering through excitation of crustal fluids (Hill and Prejean 2015). When the seismicity is triggered by frictional failure, the dynamic stresses exceed the frictional strength of the remotely activated faults, which eventually causes local slip and earthquakes (Hill and Prejean 2015). According to the second model, fluid transport and pore pressure changes caused by the transient passage of surface waves decrease the effective normal stress, triggering seismicity (Beeler et al. 2000; Cocco and Rice 2002; Hill and Prejean 2015). Sometimes the remotely triggered earthquakes occur hours to days after the mainshock, rather than (only) immediately after its occurrence (e.g., Pollitz et al. 2012). However, the mechanisms behind such delayed triggering remain less known (Parsons 2005).

Harrington and Brodsky (2006) reported that the occurrence of remote, dynamically triggered seismicity in Japan is relatively scarce compared to that in California or Greece, which is often found in locally extensional environments, and proposed that the compressional tectonics of Japan and the frequent occurrence of large mainshocks might inhibit the triggering. Van der Elst and Brodsky (2010) found that stress changes > ~30 kPa are required to trigger earthquakes in Japan, while earthquakes are triggered by smaller transient stresses in California (≥ ~0.1 kPa) (see also Miyazawa et al. 2021). However, there have been several more recent observations of dynamic triggering in Japan which provided new insights into the mechanism of triggering. Thus, Miyazawa (2011) found widespread early post-mainshock earthquakes triggered by the passage of the surface wave front from the 2011 M_w9.0 Tohoku–Oki earthquake. Enescu et al. (2016) reported a relatively widespread activation of dynamically triggered seismicity in Japan following the 2016 M_w7.1 Kumamoto earthquake. In particular, triggered seismicity was found at or near volcanic/geothermal regions, suggesting that fluids may have an important role in the triggering process. Takeda et al. (2024) reported an increase in the triggering ability of earthquakes in the northern part of Japan, for teleseismic events that occurred after the 2011 Tohoku–Oki earthquake; the authors suggested that the megathrust earthquake might have changed the triggering environment, in particular at volcanoes in northern Japan.

The 2024 M_w 7.5 Noto earthquake, which occurred on a reverse fault in the northern part of Noto Peninsula, is one of the largest intraplate events recorded in Japan. The mainshock initiated in a region with intense earthquake swarms and ruptured bilaterally for a total distance of up to 150 km (Okuwaki et al. 2024; Fujii and Satake 2024; Ma et al. 2024; Peng et al. 2024). Ding et al. (2024) reported possible evidence of remotely triggered deep tectonic tremor along the southwest Japan subduction zone. The purpose of this study is to investigate the remote triggering of seismicity (i.e., regular earthquakes) in Japan, following this large event. By analyzing the continuous waveforms recorded at seismic stations that are located at more than ~ 2–3 fault-lengths away from the mainshock epicenter, we find clearly triggered earthquakes in several seismically active regions. None of the dynamically triggered earthquakes are recorded in the Japan Meteorological Agency (JMA) earthquake catalog. The triggered earthquakes are predominantly observed during the passage of surface waves and located mainly in volcanic areas. We also calculate dynamic stress changes at locations where triggering has been observed and compare our findings with previous results to discuss the triggering mechanism.

2 Methods

Waveform data of the High Sensitivity Seismograph Network (Hi-net), operated by the National Research Institute for Earth Science and Disaster Resilience (NIED), were used to detect earthquakes triggered by the passage of the surface waves from the 2024 Noto mainshock. The Hi-net stations are typically installed in boreholes, at depths ≥ 100 m, which allows the detection of relatively small events due to an increased signal-to-noise ratio. The closest investigated station is located at a distance of ~ 279 km from the Noto mainshock, where the static stress change caused by the mainshock can be considered relatively small compared to the dynamic ones since the mainshock main slip ruptured bilaterally along a total fault length of ~ 150 km (e.g., Okuwaki et al. 2024), with the largest slip concentrated in a segment of ~ 90 km length. We used three-component continuous velocity waveforms, from 647 Hi-net stations (National Research Institute for Earth Science and Disaster Resilience 2019), recorded from 1 h before to 1 h after the mainshock occurrence (January 1, 2024, 16:10:22 JST). To detect local earthquakes, the waveforms were filtered with a two-way Butterworth bandpass filter for a frequency range of 10–30 Hz (e.g., Shimojo et al. 2014; Enescu et al. 2016). Such events were identified visually based on their clear P and S wave arrivals and a "t_S–t_P" time ≤ 5 s. Since most of our detected earthquakes are small and observed at just one seismic station, we have carefully checked that these events are detected on all three components, vertical, N–S and E–W, and thus they are unlikely to represent cultural or other types of seismic noise.

To visualize the surface waves and estimate dynamic stresses, the waveforms were first corrected for instrument response using the method developed by Maeda et al. (2011). We then validated the correction by comparing the surface wave amplitude of the corrected Hi-net recordings with those recorded at nearby F-net stations. After instrument correction, we applied a two-way Butterworth bandpass filter, in the frequency range of 0.01–0.2 Hz. Then, the horizontal components were rotated to obtain the transverse and radial component waveforms. To calculate the peak dynamic stress changes at each Hi-net station, we used an estimation based on the observed peak ground velocity (PGV), which has been widely used in previous analyses (e.g., Peng et al. 2009). According to Jaeger and Cook (1979), the peak dynamic stress change (σ_d) is proportional to Gu'/V_{ph}, where G is the shear modulus (30 GPa), u' is the peak particle velocity that can be measured directly from the waveforms, and V_{ph} is the phase velocity of the surface waves, considered here as 4.1 km/s for the Love waves and 3.5 km/s for the Rayleigh waves.

3 Results

Figure 1 shows the location of the Hi-net stations where triggered earthquakes are observed during the passage of surface waves from the Noto earthquake. Among the recordings at 647 Hi-net stations, triggered local earthquakes were identified with high confidence (Group A) at ten stations (green circles in Fig. 1). At least one pair of P-wave and S-wave arrivals from waveforms of these stations were identified during or immediately after the passage of surface waves from the Noto mainshock. Examples of triggered earthquakes are shown in Fig. 2. At other stations (blue circles in Fig. 1), the triggered earthquakes are more difficult to confirm (we refer to them as Group B) due to either low signal-to-noise ratio of seismograms, less clear observation of P-wave and S-wave arrivals, or a relatively high background seismicity level interfering with the correlation between the local earthquake and the surface waves (Figure S1).

Figure 3a shows the low-frequency (0.01–0.2 Hz) filtered waveforms recorded at 10 representative stations

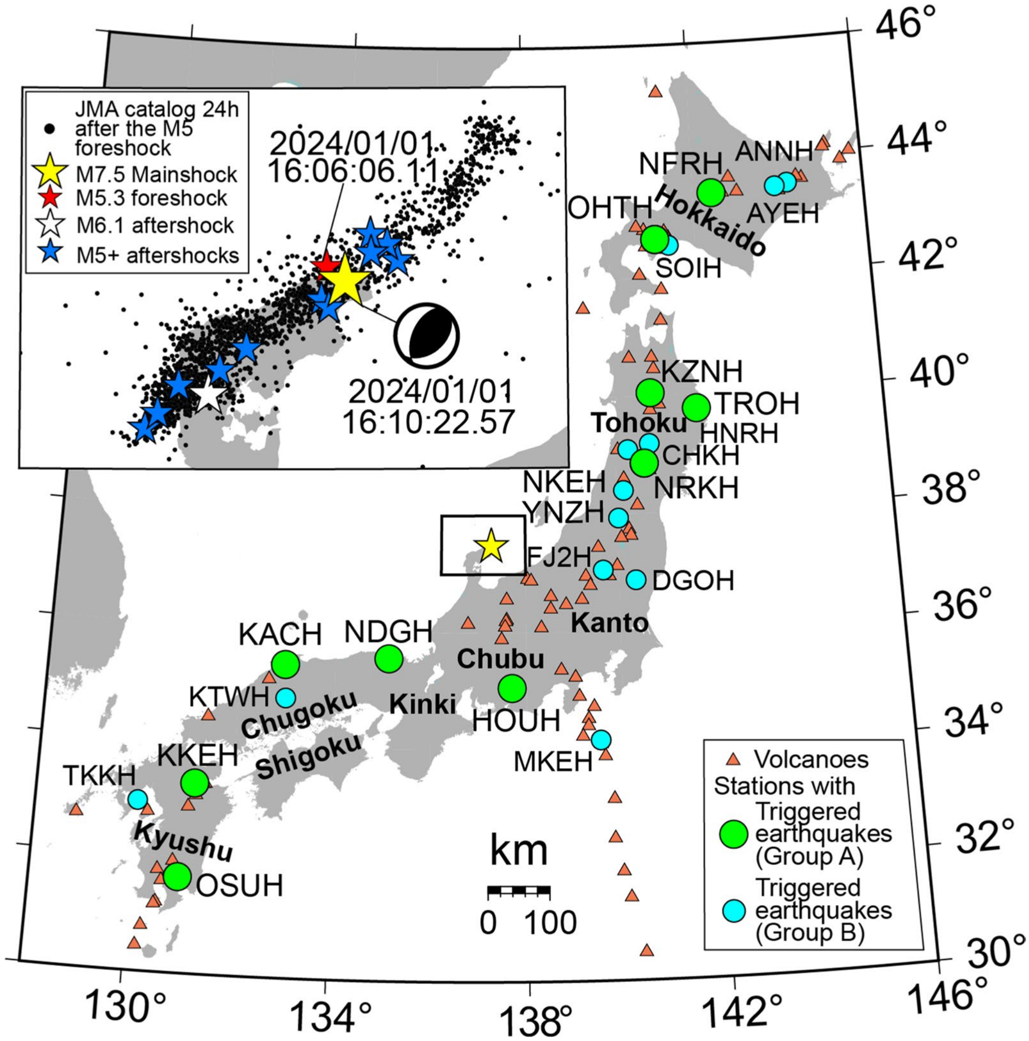

Fig. 1 Map showing the Hi-net seismic stations where triggered earthquakes were detected after the 2024 Noto earthquake. Green and blue circles show stations where clear triggered earthquakes (Group A) and less clear ones (Group B) were identified, respectively. Red triangles show volcanoes. The inset map is the zoom-in of the northern Noto Peninsula, which shows the location of the mainshock, the M5.3 foreshock, spatial distribution of the aftershocks in the first 24 h after the mainshock, and the mainshock's focal mechanism provided by the National Research Institute for Earth Science and Disaster Resilience (NIED)

(green circles in Fig. 1), after removing the instrument response. Figure 3b plots the envelope function of the vertical component of waveforms, filtered between 10 and 30 Hz; the triggered earthquakes can be identified as small, but relatively abrupt increases of the signal amplitude. Local earthquakes occurred predominantly during or after the arrival of the Noto earthquake's surface waves (Rayleigh waves, in particular) at the recording stations (Fig. 3). This observation suggests that such earthquakes are triggered dynamically by the Noto earthquake.

We then investigated the PGV for the mainshock surface waves recorded at different Hi-net stations (Fig. 4a, b). Among the ten stations (green circles in Fig. 1), the closest station to the mainshock's epicenter is HOUH, about 279 km away. At this station, the Rayleigh wave PGV is ~ 0.51 cm/s, and the Love wave PGV is ~ 0.64 cm/s. At the station NRKH located at about 332 km from the mainshock epicenter, the Rayleigh and Love waves PGVs are ~ 0.57 cm/s and 0.71 cm/s, respectively. The farthest station at which we observed triggered earthquakes in Group A is OSUH (874 km away from the mainshock). The surface wave PGVs for all Group A earthquakes are provided in Table S1. Overall, the peak surface wave PGV decreases exponentially with distance from the mainshock and both

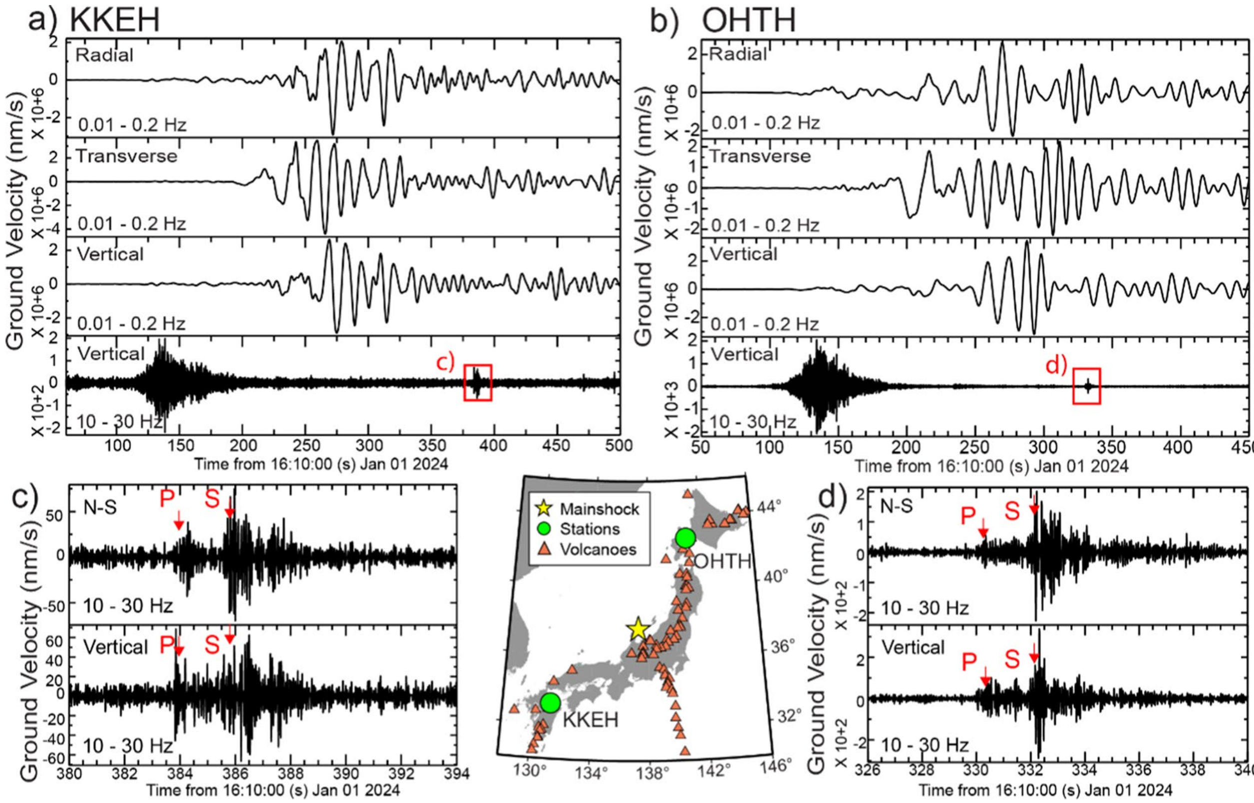

Fig. 2 Example of dynamically triggered earthquakes during the passage of the surface waves. **a** and **c** are the waveforms at station KKEH. **b** and **d** are the waveforms at station OHTH. In both **a** and **b**, from top to bottom, the top three seismograms are the radial, transverse, and vertical components which are 0.01–0.2 Hz bandpass filtered. The lowest bottom seismograms are vertical components filtered from 10 to 30 Hz. **c** Dynamically triggered earthquake in (**a**). **d** Dynamically triggered earthquake in (**b**). Central bottom shows the location of the mainshock and the two stations, KKEH and OHTH

Rayleigh and Love waves have the same exponential decay factor of − 0.002 (Fig. 4). The decay is consistent with that of Miyazawa (2011).

The estimated maximum dynamic stress change is proportional to the PGV (see Methods), which shows an exponential decrease with distance to the mainshock epicenter (Fig. 4a, b). Among the ten stations (green circles in Fig. 1), the stress change calculated from Rayleigh wave PGV varies from 16.1 kPa (OSUH) to 60.8 kPa (NDGH) and the stress change calculated from the Love wave PGV varies from 12.8 kPa (NFRH) to 52.7 kPa (NRKH). Table S1 summarizes the calculated stress change at all ten stations.

At the stations where Group B triggered earthquakes were identified, the PGVs for the Rayleigh waves are in the range of 0.20–1.20 cm/s and for the Love waves in the range of 0.13–1.22 cm/s. The dynamic stress change associated with the Rayleigh waves is in the range of 18–108 kPa and that associated with the Love waves is in the range of 10–89 kPa (Table S2).

At station NRKH, a potentially triggered earthquake is also observed during the passage of the surface waves from the M_w5.3 foreshock. The surface wave PGV and the stress change for the foreshock (Figure S2) resembles the pattern in Fig. 4, but the values are ~ 100 times smaller. The PGV for the Rayleigh waves associated with the potentially triggered earthquake is ~ 0.0016 cm/s and for the Love waves is ~ 0.0019 cm/s. The corresponding stress changes are 0.15 kPa and 0.16 kPa, for the Rayleigh waves and Love waves, respectively.

4 Discussion

4.1 Characteristics of remotely triggered earthquakes

Remote triggering of microearthquakes following the 2024 Noto mainshock are mostly observed in volcanic regions. For Group A (high confidence triggering), 11 of 14 earthquakes are observed near volcanoes. For Group B (low confidence triggering), 10 of 14 earthquakes occur near volcanoes. Among Group A earthquakes, the distances from the recording station to the nearest volcano are mostly less than 25 km (Table S1). Such a distribution

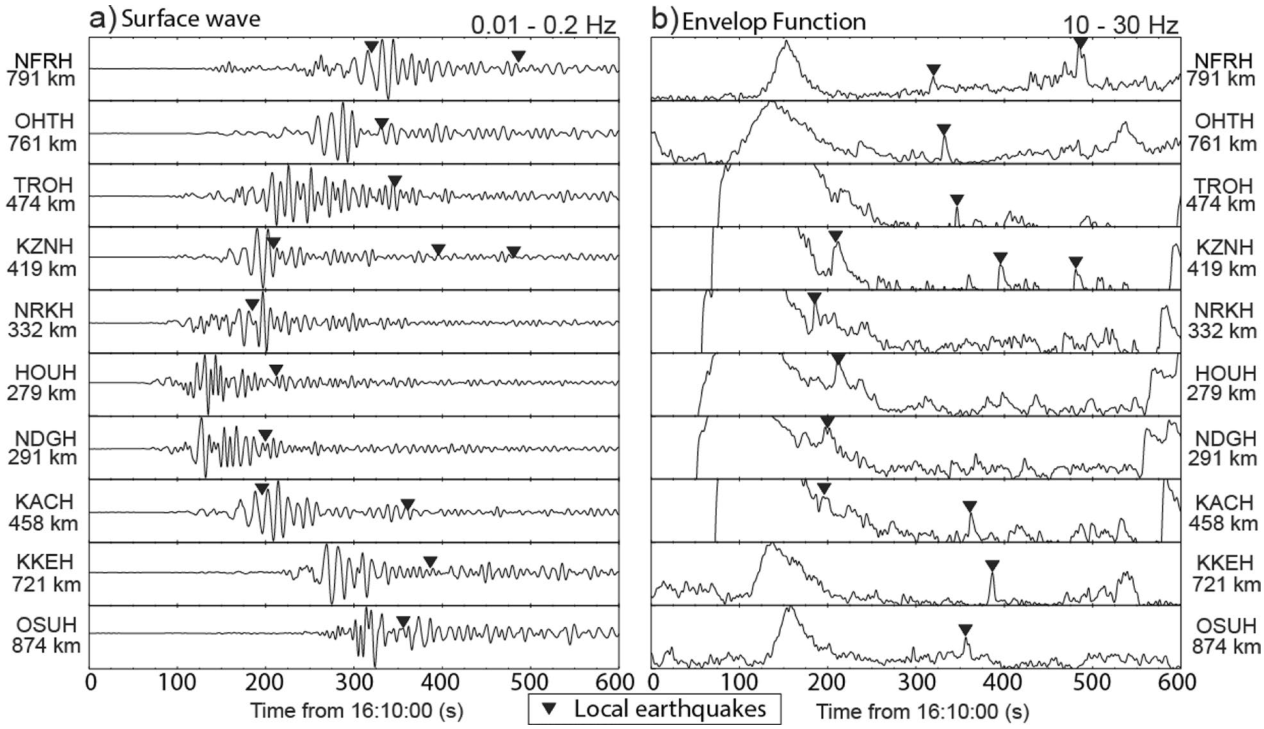

Fig. 3 Continuous waveform at Hi-net stations (Group A stations, green circles in Fig. 1), where remotely triggered earthquakes have been observed due to the passage of the surface waves from the 2024 Noto earthquake (yellow star in Fig. 1). **a** Vertical component waveforms filtered between 0.01 and 0.2 Hz that shows the passage of the surface waves. **b** Envelope function of the vertical component of waveforms filtered between 10 and 30 Hz to show the local seismicity. Inverted triangles in both (**a**) and (**b**) mark the local triggered earthquakes with "t_S–t_P" time ≤ 5 s. Station names and the distance from the station to the mainshock are also indicated

of triggered earthquakes confirms previous research that shows volcanic regions are easier to be activated dynamically, likely due to the excitation of fluids by the passage of the mainshock surface waves (Hill and Prejean 2015). In non-volcanic areas, triggered earthquakes are observed at stations TROH in northern Tohoku, HOUH in Chubu, and NDGH in Kinki region. At both HOUH and NDGH stations, triggered earthquakes were also observed during the passage of surface waves from the Kumamoto earthquake (Enescu et al. 2016). Such repeated activation may indicate faults where the state-of-stress is close to the threshold of earthquake nucleation.

The predominant frequencies of the analyzed surface waves that are responsible for triggering earthquakes in this study are around 0.05–0.2 Hz (5–20 s), with a maximum spectral amplitude of around 10 m/s/Hz (Figure S3). These predominant frequencies are consistent with those reported in the case of the triggered earthquakes following the 2016 Kumamoto earthquake (0.05–0.1 Hz; Enescu et al. 2016).

As in other dynamic triggering cases (Miyazawa 2011; Enescu et al. 2016), an earthquake triggering front is also apparent in the case of the 2024 Noto earthquake, which is consistent with the surface wave propagating front (Fig. 3). The PGV values during the surface wave arrivals for the Group A events are equal to or larger than 0.17 cm/s, similar to those observed in the case of the Kumamoto earthquake (Enescu et al., (2016), which were typically above 0.20 cm/s.

Among the Group A and B earthquakes, the minimum PGV and dynamic stress change responsible for triggering are 0.13 cm/s and 9.9 kPa (at station AYEH, Table S2), respectively. These values are similar to those reported by Enescu et al. (2016) and Takeda et al. (2024), but smaller than the values found in several other studies of triggering in Japan. For example, Harrington and Brodsky (2006) report that for the case of the 2004 Sumatra earthquake, which produced peak shaking amplitudes in the range 0.25–0.7 cm/s in Japan, only the largest PGVs were associated with some remotely triggered events. Van der Elst and Brodsky (2010) report significantly higher dynamic stress change thresholds (> ~30 kPa) for Japan. The stress changes reported in this study may support the findings of Takeda et al. (2024), who suggest that after the 2011 Tohoku–Oki earthquake the threshold of dynamic triggering at volcanoes in NE Japan may have decreased.

It is also interesting to note that the PGVs caused by the 2016 Kumamoto mainshock observed in the Noto

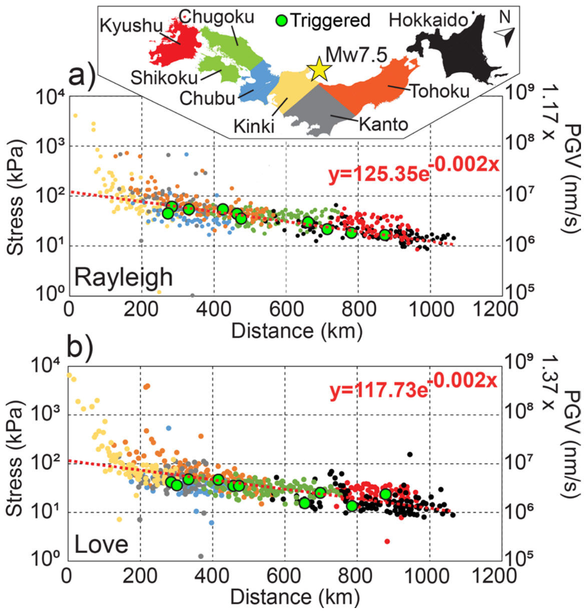

Fig. 4 Dynamic stress changes as a function of distance from the mainshock, obtained at 647 Hi-net stations. **a** Dynamic stress changes obtained for the Rayleigh waves (vertical component seismograms) and **b** obtained for the Love waves (transverse component seismograms). Color of dots indicates which area the stations belong to (e.g., red dots indicate the dynamic stress changes calculated from the waveforms recorded at the stations in Kyushu). Dashed red lines show the trend of stress change/peak ground velocity and the fitted equation, showing an exponential decay, is given at the top right corner of each graph. The left *y*-axis shows stresses (kPa), while the right *y*-axis represents the associated PGVs (nm/s). The green dots indicate the stress change at the ten stations where triggered earthquakes have been observed with good confidence (Group A)

Peninsula, which triggered earthquakes, are in the range of 0.34–0.72 cm/s (~24–56 kPa) (Enescu et al. 2016). However, in the case of the larger 2024 Noto earthquake, the observed PGV in the Kumamoto region, caused by the Noto mainshock that triggered earthquakes is in the range of 0.20–0.52 cm/s (15–38 kPa). One possible explanation is that Kumamoto earthquake is a strike-slip event, while Noto earthquake is a thrust event. Although the surface waves from both earthquakes traveled about the same distance, the 2016 Kumamoto earthquake was characterized by relatively stronger Love waves (Enescu et al. 2016), which is consistent with previous studies reporting that strike-slip events might have more energetic Love waves (Choy and Boatwright 1995; Fukao and Abe 1971). We have checked the geologic structures at the observed triggering locations and it seems that local amplification factors are unlikely to explain the PGV difference (Lopez and Ishiwatari 2002; Mukunoki et al. 2016). The relatively strong Love waves in the case of the Kumamoto earthquakes might be also responsible for the widespread seismicity activation, at distances as large as ~1650 km (Enescu et al. 2016). Similarly, a global transient increase of M > 5 events were found following the 2012 M8.6 and M8.2 Indian Ocean earthquakes, which were also large strike-slip events, highlighting the importance of Love waves in triggering small to moderate-size earthquakes (Pollitz et al. 2012).

4.2 Magnitude estimations for the triggered earthquakes

So far, we did not explicitly discuss the magnitudes of the triggered earthquakes in this paper, since, in general, they are recorded by a small number of stations and overlap on seismograms with the arrival of the mainshock surface waves. Thus, magnitude estimations may have a large degree of uncertainty and tend to be overestimated (e.g., Takeda et al. 2024). To get some rough estimates for the magnitudes, we used the earthquakes that are recorded in the JMA catalog as reference. When a triggered earthquake has the same "t_S–t_P" and same S-wave amplitude as a JMA-catalog earthquake, at a recording station, we assign the triggered earthquake the same magnitude as that of the JMA-catalog event. Most of the dynamically triggered earthquakes have magnitudes around M1.0–M1.7, with one exception of the mainshock-triggered earthquake at station NRKH, which has a magnitude of around M2.3. Since these dynamically triggered earthquakes are only recorded at a single station, the magnitude estimations should be regarded with caution. Note that none of the triggered earthquakes we detected are recorded in the JMA catalog, highlighting the importance of examining high-frequency radiations of continuous waveforms for identifying those triggered earthquakes.

4.3 Probability estimates for the triggered versus background earthquakes

We calculated an approximate probability of Group A earthquakes to be background earthquakes, using the method proposed by Stein and Wysession (2009). To define a short-term background window, we identified events on the continuous waveform recordings in a 24 h period before the occurrence of the Noto mainshock, having "t_S–t_P" times smaller than or equal to 5 s. For observations at three stations (NFRH, NDGH, KACH), for which no event was detected on the continuous waveforms on the 24 h window, we used all the events in the JMA catalog for a period of 1 month prior to the mainshock, in a 20 km × 20 km × 20 km spatial window, to define the background. At stations NFRH and KACH, since there is no earthquake recorded neither within the 24 h time window nor in the 1-month JMA catalog, we assume, for the sake of the statistical test, that there is one earthquake that occurred during the 1-month period (Table S3). We used the same approach to estimate probabilities for Group B earthquakes and present the results in the same table (Table S3). In general, we notice the small probabilities (e.g., mostly less than 2% for a 10-min window) of these earthquakes to be background events (Table S3), thus confirming their likely triggered nature. Note that the probability of observing by chance (i.e., as background events), in the triggering window, all the earthquakes reported in this study would equal the product of all the individual probabilities, which leads to a much smaller value (essentially 0).

4.4 *Possible triggering by the M_w5.3 Noto foreshock*

Four minutes before the Noto mainshock, an M_w 5.3 foreshock occurred 3 km northwest of the mainshock's epicenter. During the passage of both the foreshock and mainshock surface waves, triggered earthquakes are observed at station NRKH in the Tohoku region (Figs. 3 and S4). The PGV of the foreshock-triggered earthquake is around 300 nm/s, while for the mainshock-triggered earthquake is around 3000 nm/s (Fig. S4c, d). The calculated stress change caused by the passage of the mainshock's surface wave is around 49–53 kPa, while for the foreshock's surface wave is around 0.15–0.16 kPa (Figure S2). Because the potential foreshock-triggered event is observed at a single station, it is difficult to carry out comprehensive statistical tests to validate its identity. Simple calculations show that the probability that this earthquake is a background event, calculated using the same procedure as that explained in the previous section, for a 24 h-window before the foreshock occurrence, is very small (less than 5%).

We investigated around 90 $M_w 5.2 \pm 0.2$ earthquakes that occurred in Japan after 2011 and are approximately at the same distance from the station NRKH as the events within the Noto sequence, and found few possible triggering cases. However, due to low signal–noise ratio, only one triggered earthquake shows clear P and S arrivals (Figure S5).

To further investigate the probability of triggering by smaller earthquakes ($6 \geq M_w \geq 5$) at locations around station NRKH, we have visually inspected the seismograms during the passage of surface waves from 17 $M_w \geq 5$ Noto aftershocks, occurred within 1 month from the mainshock, following the same procedure described at Methods. The first seven $M_w \geq 5$ aftershocks occurred within a short time after the mainshock; therefore, their surface waves overlap with the mainshock's surface waves, so it is difficult to identify potential triggering on such rather complex waveforms. For the other ten aftershocks, four potential triggered earthquakes (occurred at 2024.01.02, 10:17:32; 2024.01.03, 10:54:35; 2024.01.03, 12:54:15 and 2024.01.09, 17:59:11) were observed; however, only one such event has clear P and S arrivals (Figure S6).

Cases of dynamically triggered seismicity with low stress thresholds have been previously documented (e.g., Gonzalez-Huizar et al. 2012; Takeda et al. 2024). However, these cases are rare, and therefore, further systematic analysis is needed to draw definite conclusions.

4.5 Seismicity changes according to the Japan Meteorological Agency (JMA) catalog

We have also visually inspected the JMA earthquake catalog to check for any significant changes in seismicity 1 day (Figure S7a) and 1 h (Figure S7b) before and after the 2024 Noto earthquake. A clear increase in seismicity occurred around 100 km southeast of the mainshock close to the Midagahara volcano in Chubu (Figure S7a). Within 24 h after the Noto earthquake, 22 earthquakes occurred in this region, while within 24 h before the mainshock there were no earthquakes in this area. Among the 22 earthquakes, the earliest and largest earthquake is an M4.0 event that occurred around 30 min after the mainshock (Figure S7c). We calculated the static stress change in this area on specific receiver faults using the slip model estimated by Okuwaki et al. (2024) and the algorithm of Wang et al. (2021). The receiver fault is chosen based on the location of the observed seismicity increase, with fault information (strike, dip, rake) provided by the National Institute of Advanced Industrial Science and Technology of Japan (https://gbank.gsj.jp/activefault/search). In the Midagahara volcanic area, the static stress change has values from ~ 40 to 70 kPa (as estimated for various depths from 8 to 18 km), which is smaller than the dynamic stress change (more than 100 kPa) estimated for this area. Nevertheless, since we did not observe any instantaneous triggering following the mainshock for this area we hypothesized that the triggering is more likely static (Belardinelli et al. 2003). However, secondary processes, including fluid excitation or damages in the fault zone frictional contact, may cause delayed dynamic triggering (e.g., Parsons 2005; Pollitz et al. 2012; Shelly et al. 2011), which, therefore, may not be ruled out. Farther from the epicentral region, no other obvious increase is found. In the Tohoku and Hokkaido volcanic areas (Figure S7a), the earthquakes that occurred after the Noto mainshock are more numerous than before the mainshock. However, the trend is less significant compared with the increase in the Midagahara volcanic area.

We were also interested in the longer-term activation pattern following the 2024 Noto earthquake. To check the activation (or relative quiescence) of seismicity, we adopted a more elaborate statistics and calculated the β-values following the same approach as Reasenberg and Simpson (1992). The β-values were computed for whole Japan, at the nodes of a grid with a spacing of 0.05 degrees, for a period of 30 days before and after the Noto mainshock. Earthquakes used are shallow (depth $\leq$ 20) inland earthquakes and offshore earthquakes on the SE side of Japan Sea, with magnitudes M $\geq$ 1.0. For each grid node, we searched for the 50 closest nearby events and computed the β-value statistics. The maximum radius at each grid point is limited to 10 km. We considered the β-values to be statistically significant if they are larger or equal than a threshold, chosen here as a rather conservative value of 3.0, to eliminate spurious detections (e.g., Pankow and Kilb 2020). Figure 5a, b presents maps with the earthquake epicentral distribution and β-value, respectively. The β-value statistics should be interpreted cautiously when comparing non-Poisson sequences (Reasenberg and Simpson 1992); however, it does correctly identify two areas of clear seismicity change (Fig. 5b). Noto Peninsula is obviously activated, since it is the aftershock area of the 2024 Noto earthquake (Fig. 5c). The Akita–Yakeyama volcanic area in Tohoku region also has a clear seismicity increase starting about 1 week after the Noto mainshock. In addition, there is a subtle seismicity increase in this region immediately following the mainshock (Fig. 5d).

4.6 Limitations of current research and improvements to be considered

In this study we have used visual inspection to identify triggered earthquakes. Recent studies (Wang et al. 2015, 2018; Yao et al. 2015, 2024) have applied machine-learning methods (e.g., Zhu and Beroza 2019) or matched-filter techniques (e.g., Peng and Zhao 2009) to produce more uniform, enhanced and objective earthquake detections. While such methods may have advantages compared to simpler visual inspection, they also have

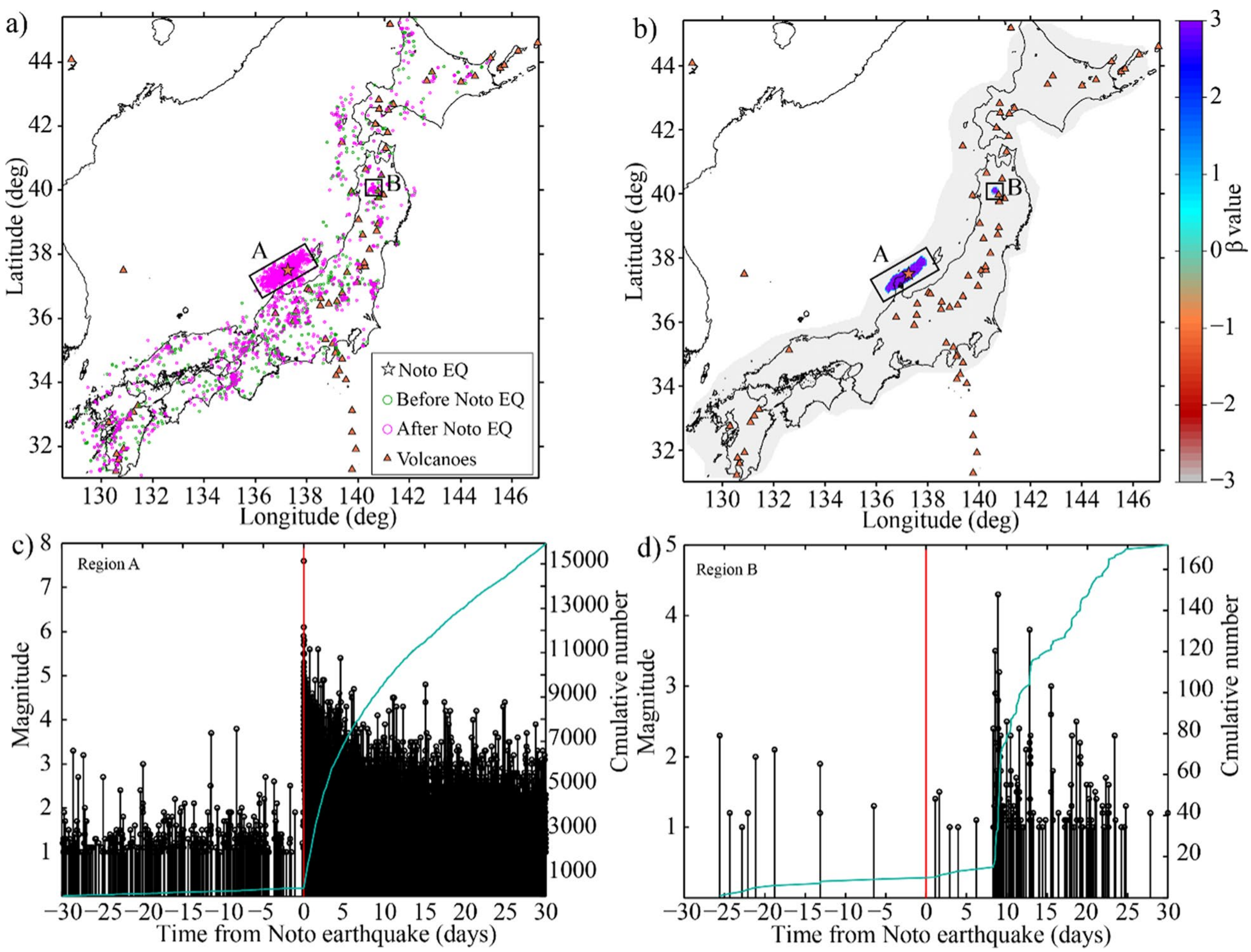

Fig. 5 **a** Epicentral distribution of inland earthquakes that occurred 30 days before and after the 2024 Noto earthquake. **b** β-value calculated using the same earthquakes shown in (**a**). Gray areas represent regions where the β-value cannot be calculated, using the conditions indicated in the text. **c** Cumulative number of earthquakes that occurred 30 days before and after the 2024 Noto mainshock in region A, Noto peninsula. **d** Cumulative number of earthquakes that occurred 30 days before and after the 2024 Noto earthquake mainshock in region B, northern Tohoku

requirements that might be sometimes difficult to fulfill, like proper training using local data for the machine learning algorithms and availability of events that can be used as templates for the matched-filter techniques. Improvements of using latest techniques to quantify dynamic triggering (e.g., Wang et al. 2018; Miyazawa et al. 2021; DeSalvio and Fan 2023) and estimate the dynamic stress changes (e.g., Yoshida et al. 2020) should also be considered.

5 Conclusions

We report remote triggering of seismicity following the M_w 7.5 Noto earthquake occurred on January 1st, 2024, in Noto Peninsula. Our analysis shows a clear correlation between the passage of the surface wave from the Noto mainshock and remotely activated seismicity, thus mostly reflecting their instantaneous triggering behavior. Most triggered earthquakes occur at or near volcanic areas, suggesting that fluids may have promoted triggering by lowering normal stresses and facilitating fault slip. Some of the volcanic regions, such as Akita–Komagatake (northern Tohoku), have also experienced triggering following the 2016 M_w 7.1 Kumamoto earthquake and/or other large teleseismic events (Enescu et al. 2016; Takeda et al. 2024). The PGVs at the triggered earthquake sites are in the range of 0.15 to 1.41 cm/s and the calculated dynamic stress change is in the range of 12.8 to 102.6 kPa. The minimum PGVs and dynamic stress changes support previous findings reported for Japan. We also found potential dynamic triggering by the Noto foreshock (M_w 5.3), at levels of stress about 100 times smaller; however, it is difficult to rigorously confirm it statistically. The analysis of a longer-term (1 month) seismicity pattern, based on the JMA earthquake catalog, revealed one remote volcanic area (Akita–Yakeyama), located about 419 km from the Noto mainshock that showed a statistically significant increase in seismicity. We hypothesize that this activation may relate to the Noto earthquake, since immediate dynamic triggering is also observed in the same region. Such possible long-term activations should be further studied and the areas involved carefully monitored, as they may help understand the underlying physical mechanisms and the seismic hazard in the activated areas.

Abbreviations

JMA	Japan Meteorological Agency
Hi-net	High Sensitivity Seismograph Network
NIED	National Research Institute for Earth Science and Disaster Resilience
USGS	United States Geological Survey
PGV	Peak ground velocity

Supplementary Information

The online version contains supplementary material available at https://doi.org/10.1186/s40623-024-02127-z.

Supplementary Material 1.

Acknowledgements

The authors would like to thank Professors Keiko Kuge, Yoshihiro Kaneko, Makiko Ohtani and all Seismology Lab members for support during the elaboration of this work. We thank NIED for providing the Hi-net data used in this study. L.A. is supported by the JST SPRING, Grant Number JPMJSP2110. B. E. is grateful to the NUCLEU Program SOL4RISC, Project no PN23360201, supported by MCID. M.M. thanks the Ministry of Education, Culture, Sports, Science, and Technology (MEXT) of Japan under its "The Second Earthquake and Volcano Hazards Observation and Research Program (Earthquake and Volcano Hazard Reduction Research)". Z.P. is partially supported by NSF Grants CAIG-2425889, EAR-1925965 and EAR-2425889. Maps were prepared using Generic Mapping Tools (Wessel et al. 2019). Waveform analysis was carried out using the Seismic Analysis Code (Goldstein et al. 2003). Statistical analysis was carried out using the ZMAP software package (Wiemer 2001). We are grateful to the three anonymous reviewers for insightful comments and suggestions and the Editor, Professor Naoki Uchida, for the fast handling of the manuscript.

Author contributions

L.A. and B.E. designed, conceived and wrote the manuscript. Z.P. proposed the estimation of static stress changes for the Midagahara region and the calculation of the probability for the foreshock triggering. M.M. proposed the use of the β-value statistic for the longer-term activation of seismicity. H.G.H gave indications for the analysis of dynamic stresses. Y. I. proposed the inclusion of the JMA catalog into the analysis. All the authors contributed to the scientific discussion and the drafting of the manuscript.

Funding

This research is supported by the JST SPRING, Grant Number JPMJSP2110, the JSPS KAKENHI Grant Number JP21H05206 in Transformative Research Areas (A) Science of Slow to Fast Earthquakes and the NSF CAIG-2425889 Grant.

Availability of data and materials

Waveform data presented in this study are available through Hi-net website: (https://hinetwww11.bosai.go.jp/auth/download/cont/?LANG=ja).

Declarations

Ethics approval and consent to participate

Not applicable.

Consent for publication

Not applicable.

Competing interests

We declare no competing interests.

Author details

[1]Department of Geophysics, Graduate School of Science, Kyoto University, Kyoto, Japan. [2]National Institute for Earth Physics, Bucharest, Romania. [3]School of Earth and Atmospheric Sciences, Georgia Institute of Technology, Atlanta, GA, USA. [4]Disaster Prevention Research Institute, Kyoto University, Uji, Kyoto, Japan. [5]Departamento de Sismología, Centro de Investigación Científica y de Educación Superior de Ensenada, Baja California (CICESE), Ensenada, Mexico.

Received: 25 June 2024 Accepted: 15 December 2024
Published online: 30 December 2024

References

Aiken C, Peng Z (2014) Dynamic triggering of microearthquakes in three geothermal/volcanic regions of California. J Geophys Res 119:6992–7009. https://doi.org/10.1002/2014JB011218

Beeler N, Simpson R, Hickman S, Lockner D (2000) Pore fluid pressure, apparent friction, and Coulomb failure. J Geophys Res 105(B11):25533–25542. https://doi.org/10.1029/2000JB900119

Belardinelli ME, Bizzarri A, Cocco M (2003) Earthquake triggering by static and dynamic stress changes. J Geophys Res 108:2135. https://doi.org/10.1029/2002JB001779

Brodsky EE, Karakostas V, Kanamori H (2000) A new observation of dynamically triggered regional seismicity: earthquakes in Greece following the August, 1999, Izmit, Turkey earthquake. Geophys Res Lett 27:2741–2744. https://doi.org/10.1029/2000GL011534

Choy GL, Boatwright JL (1995) Global patterns of radiated seismic energy and apparent stress. J Geophys Res 100:18205–18228. https://doi.org/10.1029/95JB01969

Cocco M, Rice JR (2002) Pore pressure and poroelasticity effects in Coulomb stress analysis of earthquake interactions. J Geophys Res 107:B2. https://doi.org/10.1029/95JB01969

DeSalvio ND, Fan W (2023) Ubiquitous earthquake dynamic triggering in southern California. J Geophys Res. https://doi.org/10.1029/2023JB026487

Ding C, Peng Z, Yao D, Obara K, Enescu B (2024) Comparison of multiple methods to identify remotely triggered tremor and their applications in Japan following the 2024 M_w 7.5 Noto Earthquake. In: Poster presented at the 2024 Seismological Society of American Annual Meeting, 29 April–3 May, Anchorage, Alaska. 2024

Enescu B, Shimojo K, Opris A, Yagi Y (2016) Remote triggering of seismicity at Japanese volcanoes following the 2016 M 7.3 Kumamoto earthquake. Earth Planets Sp 68:165. https://doi.org/10.1186/s40623-016-0539-5

Fan W, McGuire JJ, Shearer PM (2020) Abundant spontaneous and dynamically triggered submarine landslides in the Gulf of Mexico. Geophys Res Lett 47(12):e2020GL087213. https://doi.org/10.1029/2020GL087213

Fujii Y, Satake K (2024) Slip distribution of the 2024 Noto Peninsula earthquake (MJMA 7.6) estimated from tsunami waveforms and GNSS data. Earth Planets Sp 76:44. https://doi.org/10.1186/s40623-024-01991-z

Fukao Y, Abe K (1971) Multi-mode Love waves excited by shallow and deep earthquakes. Bull Earthq Res Inst 49:1–12

Goldstein P, Dodge D, Firpo M, Minner L (2003) "SAC2000: signal processing and analysis tools for seismologists and engineers. In: Lee WHK, Kanamori H, Jennings PC, Kisslinger C (eds) Invited contribution to "The IASPEI international handbook of earthquake and engineering seismology." Academic Press, London

Gomberg J, Reasenberg P, Bodin P, Harris RA (2001) Earthquake triggering by seismic waves following the Landers and Hector Mine earthquakes. Nature 411:462–466. https://doi.org/10.1038/35078053

Gomberg J, Bodin P, Larson K, Dragert H (2004) Earthquakes nucleated by transient deformations caused by the M 7.9 Denali Alaska, earthquake. Nature 427:621–624. https://doi.org/10.1038/nature02335

Gonzalez-Huizar H, Velasco AA, Peng Z, Castro RR (2012) Remote triggered seismicity caused by the 2011, M9.0 Tohoku-Oki, Japan earthquake. Geophys Res Lett 39(10):L10302. https://doi.org/10.1029/2012GL051015

Harrington RM, Brodsky EE (2006) The absence of remotely triggered seismicity in Japan. Bull Seismol Soc Am 96:871–878. https://doi.org/10.1785/0120050076

Hill DP, Prejean SG (2015) Dynamic triggering. In: Kanamori H, Schubert G (eds) Treatise on geophysics, vol 4. Elsevier, Amsterdam, pp 273–304

Hill P, Reasenberg PA, Michael A, Arabaz WJ, Beroza G, Brumbaugh D, Brune JN, Castro R, Davis S, dePolo D, Ellsworth WL, Gomberg J, Harmsen S, House L, Jackson SM, Johnston MJS, Jones L, Keller R, Malone S, Munguia L, Nava S, Pechmann JC, Sanford A, Simpson RW, Smith RB, Stark M, Stickney M, Vidal A, Walter S, Wong V, Zollweg J (1993) Seismicity remotely triggered by the magnitude 7.3 Landers California, earthquake. Science 260:1617–1623. https://doi.org/10.1126/science.260.5114.1617

Hough SE, Seeber L, Armbruster JG (2003) Intraplate triggered earthquakes; observations and interpretation. Bull Seismol Soc Am 93:2212–2221. https://doi.org/10.1785/0120020055

Jaeger JC, Cook NGW (1979) Fundamentals of rock mechanics, 3rd edn. Chapman and Hall, London

King GCP, Stein RS, Lin J (1994) Static stress changes and the triggering of earthquakes. Bull Seismol Soc Am 84(3):935–953. https://doi.org/10.1785/BSSA0840030935

Lopez JC, Ishiwatari A (2002) Petrogenesis of the tholeiitic basalt, calc-alkaline basaltic andesite and high magnesian andesite lava succession of the Oligo-Miocene Anamizu Formation in northeastern Noto Peninsula, central Japan. J Miner Petrol Sci 97(3):85–113. https://doi.org/10.2465/jmps.97.85

Ma Z, Zeng H, Luo H, Liu Z, Jiang Y, Aoki Y, Wang W, Itoh Y, Lyu M, Cui Y, Yun SH, Hill EM, Wei SJ (2024) Slow rupture in a fluid-rich fault zone initiated the 2024 Mw 7.5 Noto earthquake. Science. https://doi.org/10.1126/science.ado5143

Maeda T, Obara K, Furumura T, Saito T (2011) Interference of long-period seismic wavefield observed by the dense Hi-net array in Japan. J Geophys Res 116:B10303. https://doi.org/10.1029/2011JB008464

Miyazawa M (2011) Propagation of an earthquake triggering front from the 2011 Tohoku-Oki earthquake. Geophys Res Lett 38:L23307. https://doi.org/10.1029/2011GL049795

Miyazawa M (2012) Detection of seismic events triggered by P-waves from the 2011 Tohoku-Oki earthquake. Earth Planets Sp 64:1223–1229. https://doi.org/10.5047/eps.2012.07.003

Miyazawa M, Brodsky EE, Guo H (2021) Dynamic earthquake triggering in southern California in high resolution: Intensity, time decay, and regional variability. AGU Adv 2:e2020AV000309. https://doi.org/10.1029/2020AV000309

Mukunoki T, Kasama K, Murakami S, Ikemi H, Ishikura R, Fujikawa T, Yasufuku N, Kitazono Y (2016) Reconnaissance report on geotechnical damage caused by an earthquake with JMA seismic intensity 7 twice in 28 h, Kumamoto, Japan. Soils Found 56(6):947–964. https://doi.org/10.1016/j.sandf.2016.11.001

National Research Institute for Earth Science and Disaster Resilience (2019) NIED Hi-net, National Research Institute for Earth Science and Disaster Resilience, https://doi.org/10.17598/NIED.0003

Okuwaki R, Yagi Y, Murakami A, Fukahata Y (2024) A multiplex rupture sequence under complex fault network due to preceding earthquake swarms during the 2024 Mw 7.5 Noto Peninsula, Japan, Earthquake. Geophys Res Lett 51:e2024GL109224

Opris A, Enescu B, Yagi Y, Zhuang J (2018) Triggering and decay characteristics of dynamically activated seismicity in Southwest Japan. Geophys J Int 212(2):1010–1021. https://doi.org/10.1093/gji/ggx456

Pankow KL, Kilb D (2020) Going beyond rate changes as the sole indicator for dynamic triggering of earthquakes. Sci Rep 10:4120. https://doi.org/10.1038/s41598-020-60988-2

Parsons T (2005) A hypothesis for delayed dynamic earthquake triggering. Geophys Res Lett 32:L04302. https://doi.org/10.1029/2004GL021811

Peng Z, Zhao P (2009) Migration of early aftershocks following the 2004 Parkfield earthquake. Nat Geosci 2:877–881. https://doi.org/10.1038/ngeo697

Peng Z, Vidale JE, Wech AG, Nadeau RM, Creager KC (2009) Remote triggering of tremor along the San Andreas fault in central California. J Geophys Res 114:B00A06. https://doi.org/10.1029/2008JB006049

Peng Z, Lei X, Wang Q-Y, Wang D, Mach P, Yao D, Kato A, Obara K, Campillo M (2024) The evolution process between the Earthquake Swarm Beneath the Noto Peninsula, Central Japan and the 2024 M 75 Noto Hanto Earthquake Sequence. Earthq Res Adv. https://doi.org/10.1016/j.eqrea.2024.100332

Perfettini H, Avouac J-P (2004) Stress transfer and strain rate variations during the seismic cycle. J Geophys Res 109:B06402. https://doi.org/10.1029/2003JB002917

Pollitz F, Stein R, Sevilgen V, Bürgmann R (2012) The 11 April 2012 east Indian Ocean earthquake triggered large aftershocks worldwide. Nature 490:250–253. https://doi.org/10.1038/nature11504

Reasenberg PA, Simpson RW (1992) Response of regional seismicity to the static stress change produced by the Loma Prieta Earthquake. Science 255:1687–1690. https://doi.org/10.1126/science.255.5052.1687

Shelly D, Peng Z, Hill D, Chastity A (2011) Triggered creep as a possible mechanism for delayed dynamic triggering of tremor and earthquakes. Nat Geosci 4:384–388. https://doi.org/10.1038/ngeo1141

Shimojo K, Enescu B, Yagi Y, Takeda T (2014) Fluid-driven seismicity activation in northern Nagano region after the 2011 M9.0 Tohoku-oki earthquake. Geophys Res Lett 41:7524–7531. https://doi.org/10.1002/2014GL061763
Stein S, Wysession M (2009) An introduction to seismology, earthquakes, and earth structure. Wiley-Blackwell, Oxford
Takeda Y, Enescu B, Miyazawa M, An L (2024) Dynamic triggering of earthquakes in northeast Japan before and after the 2011 M 9.0 Tohoku-Oki Earthquake. Bull Seismol Soc Am 114(4):1884–1901. https://doi.org/10.1785/0120230051
van der Elst NJ, Brodsky EE (2010) Connecting near-field and far-field earthquake triggering to dynamic strain. J Geophys Res. https://doi.org/10.1029/2009JB006681
Velasco A, Hernandez S, Parsons T (2008) Global ubiquity of dynamic earthquake triggering. Nat Geosci 1:375–379. https://doi.org/10.1038/ngeo204
Wang W, Meng X, Peng Z, Chen Q, Liu N (2015) Increasing background seismicity and dynamic triggering behaviors with nearby mining activities around Fangshan Pluton in Beijing, China. J Geophys Res 120:5624–5638. https://doi.org/10.1002/2015JB012235
Wang B, Harrington RM, Liu Y, Kao H, Yu H (2018) Remote dynamic triggering of earthquakes in three unconventional Canadian hydrocarbon regions based on a multiple-station matched-filter approach. Bull Seismol Soc Am 109(1):372–386. https://doi.org/10.1785/0120180164
Wang J, Xu C, Freymueller JT, Wen Y, Xiao Z (2021) AutoCoulomb: an automated configurable program to calculate coulomb stress changes on receiver faults with any orientation and its application to the 2020 7.8 Simeonof Island, Alaska, Earthquake. Seismol Res Lett 92(4):2591–2609. https://doi.org/10.1785/0220200283
Wessel P, Luis JF, Uieda L, Scharroo R, Wobbe F, Smith WHF, Tian D (2019) The generic mapping tools version 6. Geochem Geophys Geosy 20:5556–5564. https://doi.org/10.1029/2019GC008515
Wiemer S (2001) A software package to analyze seismicity: ZMAP. Seismol Res Lett 72(3):373–382. https://doi.org/10.1785/gssrl.72.3.373
Yao D, Peng Z, Meng X (2015) Systematical search for remotely triggered earthquakes in Tibetan Plateau following the 2004 M 9.0 Sumatra and 2005 M 8.6 Nias earthquakes. Geophys J Int 201(2):543–551. https://doi.org/10.1093/gji/ggv037
Yao D, Ding C, Peng Z, Sandvol E, Godoladze T, Yetermishli G (2024) Dynamically triggered tectonic tremors and earthquakes in the Caucasian region following the 2023 Kahramanmaraş, Türkiye, Earthquake Sequence. Geophys Res Lett. https://doi.org/10.1029/2024GL110786
Yoshida S, Maeda T, Kato, N (2020) Earthquake triggering model based on normal-stress-dependent Nagata law: application to the 2016 Mie offshore earthquake. Earth Planets Sp 72:141. https://doi.org/10.1186/s40623-020-01272-5
Yukutake Y, Miyazawa M, Honda R, Harada M, Ito H, Sakaue M, Koketsu K, Yoshida A (2013) Remotely triggered seismic activity in Hakone volcano during and after the passage of surface waves from the 2011 M9.0 Tohoku-Oki earthquake. Earth Planet Sci Lett 373:205–216. https://doi.org/10.1016/j.epsl.2013.05.004
Zhu W, Beroza GC (2019) PhaseNet: a deep-neural-network-based seismic arrival-time picking method. Geophys J Int 216(1):261–273. https://doi.org/10.1093/gji/ggy423

Publisher's Note